Journal of Network and Innovative Computing
ISSN 2160-2174 Volume 1 (2013) pp. 248-259


# Texture Classification of Biased Cytoplasmic Tissue Sample from Histopathological Imagery by Gabor Application

Pranshu Saxena[1], Sanjay Kumar Singh[2] and Prateek Agrawal[3]

[1]Department of Computer Science Engineering
Lovely Professional University, Jalandhar, India
*pranshusaxena@gmail.com*

[2]Department of computer science Engineering
Lovely Professional University, Jalandhar, India
*sanjayksingh.012@gmail.com*

[3]Department of computer science Engineering
Lovely Professional University, Jalandhar, India
*prateek061186@gmail.com*

***Abstract*: Recent research with H&E stained imagery led to rapid progress towards quantifying the perceptive issues, while prognostic, due to subjective variability among readers. This variability leads to distinguish prognosis report and variability in treatment as well. So in this study we present thoughtful analysis of texture heterogeneity on Follicular Lymphoma and Neuroblastoma tissue images for the purpose of identifying regions of interest in tissue for morphological behavior. We are introducing a classification approach for determining the texture feature i.e. described by parameters like nuclei, cytoplasm, extracellular material and red blood cells and the subsequent classification of histopathological digital image. Basic idea behind this research is to distinguish among nuclei, cytoplasm, extracellular material and red blood cells from H&E stained input image so that doctors (radiologist) can provide better judgment during the prognosis of histopathological image that sometimes wrongly concluded (even though educated).**

**In this memorandum we proposed a noble algorithm in which we convolve our H&E stained pathological images with 12 different orientation masks (masks obtained from Gabor application), resulting in an outputs of 12 different representations (corresponding to 12 different orientations masks) of our H&E stained input image i.e. the information included in the 12 representations coming from the application of Gaussian filter is summarized in twelve images that correspond to each of the orientations used in the filters. We then combine these 12 images into one textured image represented as a 3-dimensional representation of input image. Experimental results on FL & NB demonstrate that the proposed approach outperforms the gray level based texture analysis.**

***Index Items:*** Computer-aided diagnosis, follicular lymphoma, gabor mask, gaussian wavelet, image classification, neuroblastoma, texture analysis**.**

## I. Introduction

Follicular Lymphoma (FL) is one of the most common non-Hodgkin B-cell lymphomas in the world with a highly variable clinical course and Neuroblastoma (NB), cancer of nerve cell origin and it commonly affects infants and children. Based on the American Cancer Society's (ACS) statistics, it is by far the most common cancer in infants and the third most common type of cancer in children [1], [2]. The samples of these fatal diseases are included in our research and experimented. The idea of taking both diseased parallel is similarity in their representation [2]. Patients suffering with FL & NB do not get benefitted by early therapy. In fact, early chemotherapy for their treatment may cause more harms than benefits; therefore should be avoided. On the other hand, FL & NB patients with aggressive disease short survival, if not treated properly i.e. should receive appropriate therapy as soon as possible to increase their chance of re-mission and to prolong their lives. These important clinical decisions are currently guided by histological grading of the tumor.

As recommended by the World Health Organization (WHO)[11], histopathological grading of FL is based on the number of large malignant cells, namely Centro blasts (CB), per standard 40× magnifications high power microscopic field (HPF) of 0.159 $mm^2$ [3]. In this method, Centro blasts are manually counted and the average of CB/HPF [11] is reported. And according to WHO, high power fields (HPF) of hematoxilin and eosin (H&E) stained tissue sections (under microscope) are classify the biopsy into one of the three histopathological grades according to the average CB count per HPF. Grades I specifies (0–5 CB/HPF) and Grade II (6–15CB/HPF) are considered low risk categories while Grade III (>15CB/HPF) is considered a high risk category.

This clinical relevance of grading system is still being debated; Grade I, II, III/A are considered to be indolent and incurable while Grade III/B is belongs to most aggressive but curable [35]. In the above classification Grade I & II belongs to quantitative issue (count the number of CB/HPF) while classification of Grade III in its respective subgroups required qualitative issue as CB/HPF remain same (>15 in both cases Grade III A, B). Only subjective issue which distinguished between Grade IIIA & B is that IIIA shows that centrocytes still present, whereas in IIIB the follicles consists almost entirely of Centro blast [35]. Although patients suffering with indolent FL (Grade I, II, III) typically live for many decades with minimal or no treatment while patients with aggressive FL has short survival if not treated appropriately at early stages.

In the context of Neuroblastoma the WHO recommends the use of the International Neuroblastoma Pathology Classification (the Shimada system) for categorization of the patients into different prognostic groups [1], [7], [39]. That classification system based on morphological characteristics of the tissue Figure 1 shows a relevant summary of this classification system as a tree diagram [39]. The histopathological examination guides the oncologists in making decisions on time and on the required therapy;

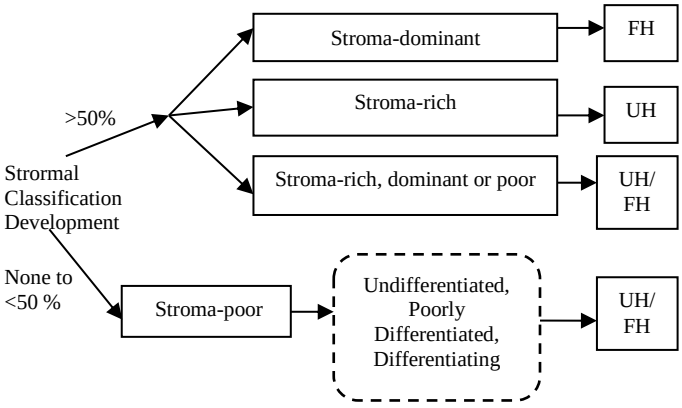


**Figure 1**. A simplified diagram of the international neuroblastoma pathology classification (the Shimada System) into unfavorable and favorable histology

In the current scenario for practical reasons, pathologists typically count CB's that may be possible consequences of over or under grading of FL and NB as well includes inappropriate timing and type of therapy with serious clinical consequences for patients. Moreover the accuracy of the classification is important to prevent making any under or over treatment. Unfortunately, this classification becomes more vulnerable when oncologist prognostic these highly microscopic (e.g. 40x) biopsy by only picking a small representative section (e.g. 2x or 4x) and concluded for a whole slide (40x) tissue sample and sometimes subjectivity issue also conquered among different readers. This subjectivity and variability of manual grading does affect the accuracy of diagnosis and success of the treatment.

Therefore we are focusing on to provide distinguished representation for each element (nuclei, cytoplasm, extracellular material and red blood cell) from H&E stained input image so that subjectivity between oncologists can be reduces. We are not counting the CB/HPF in this research paper. Proposed algorithm is able to represent each Centro blast elements of input image with different color. This different representation in color leads us to describe a new quality parameter called texture analysis, which refers to the characterization of regions in an image by their texture content. In other words it's a repetition of an element or pattern on the surface [8]. Texture analysis attempts to quantify intuitive qualities described by terms such as rough, smooth, silky or bumpy as function of the spatial variation in pixel intensities and to extract boundary between major texture regions.

There are many techniques that are used for the extraction of features: statistical methods (grey level co-occurrence matrix, grey level difference vector), filtering techniques (energy filters), wavelet decomposition-based methods, etc.

In this study, we focus on analyzing some of the Gabor function application techniques for the characterization of textures that create very different kind of environments for histopathological image, by visualizing each object of image with all possible angles and plotted a 3-Dimensional image. This technique is entirely different form the scheme proposed by S. Kothari *et al.* 2013 [43] based on shaped based feature to classified the lymphomas in their respective grades. The rest of the paper is organized as follows: Section II describes our data collection and area of study, Section III describes about the previously deployed texture scheme, methodology we proposed in section IV, that is in particular, the cell-graph based algorithm representation. In Section IV, we have presented the experimental results followed by discussion with three experienced pathologists, and finally, in the Section V, we concluded the novelty of our proposed algorithm, followed by future aspect of research work. This paper is extended version of [42].

## II. Data Collection & Area of Study

The tests were performed using two images FL and NB and the samples are collected from the various pathology in India First, Medicare Pathology Laboratory, Pune, Second, Dr. Girishs Trividi cancer Centre, kharghar (Navi Mumbai) and Finally Dr. Rubi pathology & Medical Centre, Jhansi. We asked three experienced pathologists to extract five regions of interests from each whole-slide sample that are equivalent to one microscopic HPF, resulting in a data set of 170 images. Texture features are extracted from the image using MATLAB, on Windows XP, Intel Processor.

## III. Chromatic Texture: A Review

Actually texture is the intuitive property of surface, no strict definition about image texture, it only perceive by humans and is believe to be rich source of visualization. Rosenfeld *et al*. [15] defines texture in terms of image property like brightness, color, contrast, entropy, mean, size, slope, and complex visual

patterns composed by image elements (sub patterns). Consider an image $I : \Omega \rightarrow R$ , $\Omega$ is the image domain and the segmentation of the image into its subsequent region $R$ is depends on the local sub patterns visual property like lightness, uniformity, density, roughness, regularity, smoothness, randomness, frequency, phase, granularity etc. as a whole Levine *et al.* [16] introduced that by localizing the image criteria. Further classification of image texture into four subsequent issues is proposed by Brobatz *et al.* [36] depending upon image representation, issues are;

*First*, categorization of digital image texture based on quantitative variation among pixels values that have been numerically assigned (quantitative measurement of image parameter). This numerically computation named as *Feature Extraction.*

*Second*, to partition an image into several regions based on locally assign descriptor values. By integrating this local criterion leads to classification of an image in global discrimination, this process is named as *Texture Discrimination*.

*Third*, a finite image classification based on normal and abnormal issues to which of a predetermined number of physically defined classes belongs to homogeneous texture region.

*Forth*, Classification based on geometry of image element i.e. to reconstruct 3-D surface geometry form texture information, like an application to geographical images by satellite.

Most common multi-scale feature technique that has been widely uses are texture discrimination and texture classification. Based on these classifications a lot of texture segmentation methods has been introduced by distinguished researchers, are as follows;

L. Cohen *el.al* [18] suggested a method rely on frequency that has been used for calculating these multi scale features. The most frequently used features are Wigner distribution, Gaussian Wavelet transformation, and Gabor application, however, Wigner distribution are found to hold interference terms between different components of a signal, means little but significant variation does not affect the final outcome, resultant wrong interpretation of specified object (signal). Gabor filter are criticized for their non-orthogonally i.e. convolution between image and the filter bank are not correlated, this results information contained in Gabor image representation redundant and also affect the size of representation channels Teuner *et al*. concluded that [17]. Still, Gabor filter are used for texture segmentation [18], [19], [20], [21] and the problems for designing Gabor filters for texture segmentation is considered in [37], [17]. On the other hand, Unlike Wigner distribution, the wavelet transform is functioning a linear operation, does not produce interference terms. It possesses a capability of space localization of signal (energy which propagate through image) spectral feature. For these reasons, much interest in applications of the wavelet transform to texture analysis can be noticed recently.

Later Black *et al*. [22] proposed a noble approach called Markov random hidden (MRH) process. In this process all interaction is local; and the probability that a cell is being in a given state is entirely determined by probability for state of neighboring cells. Direct interaction occurs only between immediate neighbors. However, for global criterion effects can still occur as a result of propagation.

The link between the image energy and probability is that;

$$P \propto \exp\left(-{}^{E}/_{T}\right) \tag{1}$$

Here, T is a constant. $E$ is the Energy which propagates into image. By lowering the energy $E$ (that was generated by particular MRF) nearby the region, more likely leads to trace the boundary of that heterogeneous region.

Hidden Markov models (HMM) has a potential advantage over other texture classification and discrimination methods that is, HMM attempts to discriminate an underlying fundamental structure of an image that may not be certainly observable. Experimented results of texture discrimination using identified HMM parameters are described in Povlow *et al.* [23], showing better performance than the autocorrelation method which require much larger neighborhood, on real world images for texture property.

Another statistical approach for determining the texture feature from the image by exploiting a posteriori probability information based on the Markov random field (MRF) and Gaussian random field models German *et al.* [24]. Since probabilistic based results rely on probability density function (PDF) is not estimated correctly by the MRF, while exploiting a posteriori (Maximizing a Posteriori) estimator is uses the Gibbs random field, and provides more comprehensive result. However, Hassner *et al.* [25] added that Gibbs parameter should be assessed first for texture segmentation, as they are not known a priori.

Derin *et al.* [26] proposed a noble histogramming technique for estimating efficient Gaussian Markov random field (GMRF) parameters, these parameters are elaborated in Gurelli *et al.* [27]. Unlike previous approaches it does not require exploiting of a log likelihood function; instead of, it grounded on simple histogramming, a look-up table operation and a computation of a pseudo-inverse of a matrix with reasonable dimensions. Later Yin *et al.* [28] introduced least-square method for supervised texture segmentation scheme grounded on Kohonen Artificial Neural Network (KANN), with the help of this method we estimate the second-order MRF parameter. While Andrey *et al.* [29] use Genetic algorithm for identifying the unsupervised texture segmentation.

In 1994 era comes for color texture segmentation, *first* introduced by Panjwani *et al.* [30] using Markov Random Field. In this approach parameters are estimated from texture region by a maximum pseudo likelihood scheme and the final outcome (segmentation) is achieved by conquering all the process, that results maximize the conditional likelihood of an image. The problem of selecting neighbors during the design of color RMF is still a great impediment, area of investigating. And also facing problem that is, as number of parameter increases, which is used to define the interaction within and between color bands (neighbors), proportionally the complexity of the approach increases. Bennett *et al.* [31] is also consider MRF model is his study for segmenting the color images but the problems, while texture classification using

Markov random fields and small samples is investigated by Speis *et al.* [32], they inspected that Markov fields do not provide the precise models for textured images of many real world images and for small sample like [20 x 20] doesn't contain the enough information.

Krishnamachari *et al.* [33] proposed a new approach that has certain advantages oven single resolution analysis (MRF). They introduced noble multi-resolution approach to using Gaussian Markov random field (GMRF). In this technique parameters of lower resolution are estimated from the resolution parameters. The coarsest resolution data are first segmented and the segmentation results are propagated upward to the finer resolution.

Later in this series Clause and Jernigan [4] categories the image texture into two methods: named as Supervised and non-supervised methods. Supervised methods use filters with parameters selected from the texture features to be identified. Bovik *el al.* in 1991 [5] selected the most adequate filters, based on a prior knowledge of the image textures. The non-supervised methods are more attractive, as they generate a complete filter bank, and do not require the user to precisely define the parameters that unequivocally identify a texture. So we are using unsupervised method for abstracting the texture feature from the H&E stained image and the parameter which we selected are orientation (θ), radial frequency ($F_0$) and spatial extension (σ).

In further discussion we introduced a noble multi-resolution approach (based on above parameters) that works on Gabor application for segmenting the texture from the color medical images.

## IV. Automated Texture Analysis

The multi-oriented filter is an effective method in the field of texture analysis because it imitates the characteristics of the human visual system, which decomposes the image on the retina into several filtered images, each of which has variations in intensity within a limited range of orientations and frequency as well (Jain & Farrokhnia 1991) [19]. More over in the most of the studies the relation to the local spectrum is established through (intermediate) features that are obtained by filtering the input image with a set of two-dimensional (2-D) Gabor filter such filter is linear and local. Its convolution kernel is a product of a Gaussian and a cosine function.

Our multi-oriented Gaussian filter banks (eq. 2), which comprises of 12 different filters having different angles ranging from ($30^0$-$360^0$). The particular characteristic of passing input H&E stained image from every filter bank, resulting we have 12 different convolved images corresponding to each angle, each of the image represent its own site of view (figure.1 step 3). Later we conquer all 12 convolved images into a single covariance image because of covariance matrix is coming from every angle possible that provides radiologist a 3-D representation. This way we can able to convert time-varying 2-D histopathological images viewed as 3-D functions of space-time, and it is possible that time-varying images are represented in vision areas by a 3-D Gabor-wavelet transform, which generates a time-varying five-dimensional field (representing two spatial dimensions, spatial frequency, spatial orientation and temporal frequency)( MacLennan 1997, p. 64).

The orientation of the texture is a property whose analysis is generally of interest for plotting the different intensities and uses classification of images. Thus, the classification results obtained using the sum of the output images from filtering with the 12 filters corresponding to a determined orientation were tested.

$$\mathrm{G(mask)} = \mathrm{G30°} + \mathrm{G60°} + \mathrm{G90°} + \mathrm{G120°} + .. + \mathrm{G360°} \quad (2)$$

This above formula illustrate compete filter bank comprises of 12 mask having different angles. Implementation of mask, which depends on orientation, is explained below.

In the spatial domain, a Gabor filter consists of a complex Gaussian exponential function modulated by a sinusoidal curve

$$G(x,y) = \frac{1}{2\pi\sigma^2} exp\left[-\frac{x^2+y^2}{2\sigma^2}\right] \exp\{\mathrm{J}(2\pi F(xcos\theta + ysin\theta))\} \quad (3)$$

*Where*, σ represent as a spatial extension of the discussed filter in the spatial domain.

We divide above equation into their respective real and imagery part. Oscar & Rafael suggested that only real part is necessary to represent and reconstruct the image [10] and that can be achieved by making theoretically DC (zero frequency) response of the real part of our 2D-gabor filter is closed but not exactly zero. Thus we are imposing zero frequency on them.

$$\mathrm{Re(x,y)} = \frac{1}{2\pi\sigma^2}.exp\left[-\frac{x^2+y^2}{2\sigma^2}\right].\cos\big((2\pi(a_0x + b_0y)\big) \quad (4)$$

$$\mathrm{Img(x,y)} = \frac{1}{2\pi\sigma^2}.exp\left[-\frac{x^2+y^2}{2\sigma^2}\right].\sin\big((2\pi(a_0x + b_0y)\big) \quad (5)$$

*Here,* $a_0, b_0$ define the spatial frequencies

$$Magitude\ F_0 = \sqrt{{a_0}^2 + {b_0}^2} \quad (6)$$

$$Direction\ \ \theta = tan^{-1}\left(\frac{b_0}{a_0}\right) \quad (7)$$

Now, consider the eq.3 which consists of an exponential function along with three variables $\sigma$ (spatial extension), and $a_0$ & $b_0$ these spatial frequencies can represented in the terms of orientation θ& $F_0$ easily ($a_0 = F_0\mathrm{Cos}\theta, b_0 = F_0 sin\ \theta$).

So the final result was carried out with twelve orientations θ=(30º, 60º, 90º, 120º, 150º, 180°,210°, 240°, 270°, 300°, 330°, 360°) and one radial frequency values: $F_0$= (0.3536). This leaves us with a total of 12 filters that cover the entire frequency domain. Different standard deviation values of the Gaussian curve were tested (Chan, *et al.* 1999) [38], those being the two sets of three values used in the study $\sigma_g$ = (1.91, 3.82 and 7.63) and $\sigma_g$ = (2.86, 5.73 and 11.44). These values help us in the construction of Gabor mask.

Eq. 5 of real part of complex exponential function is used to construct the Gabor mask, each mask consists of real Eigen values. Once the mask was designed, the methodological procedure followed for extraction of texture variable and later image classification was the following (fig. 1) below explain the construction of the textured image in brief.

Gabor Filter provides information on orientation and frequency of the features. We fixed the frequency, but determine the different orientations of the texture of an image because of an image is filtered with a set of Gabor filters of the different preferred orientations and spatial frequencies that cover appropriately the spatial frequency domain, and the features obtained from a feature vector field that is further used for analysis, classification, or segmentation.

We are these following ways to achieve our final textured image;

*A. Input Image*

Let Ω be the image domain and $I : \Omega \to R$ be the color medical image. A segmentation of image $I$ can be achieved by plotting the each cytoplasmic element with different color. Spatial representation of the image $I(x, y)$, where $(x, y) \epsilon\ \Omega$ (set of all points in the domain); we have to load H&E stained image and do all the appropriate conversion needed.

*B. Gaussian Filters*

We construct 12 different masks (having $30\,°$ with respect to each other) with the help of Gabor application;

$$\mathcal{G}_{(\theta,\sigma,F_0)} = \frac{1}{2\pi\sigma^2} exp\left[-\frac{x'^2 + y'^2}{2\sigma^2}\right].\cos\big((2\pi(a_0x' + b_0y')\big) \tag{8}$$

In this formulation

$$x' = (x - \xi)cos\theta - (y - \eta)sin\theta \tag{9}$$

$$y' = (x - \xi)sin\theta + (y - \eta)cos\theta \tag{10}$$

Where, the argument $x$ and $y$ belongs to the coordinate position of a point in spatial domain and ξ, η, θ, σ, $F_0$ are the parameters whose variation leads to change in Gabor mask formulation. Parameters (ξ & η), which has the same domain Ω as a pair of (x, y), specifies the center of an interested field, parameter σ accounts for the size of interested field, and the angle parameter $\theta$ $\big(\theta\ \epsilon\ [0, 2\pi)\big)$ specifies the orientation of the normal to the parallel excitatory and inhibitory strips zone.

This formulation gives us 12 different Gabor masks; Then these filter mask was applied to the input image and the magnitude of the filtered images was obtained in the next step we convolve our input image with each of the 12 masks to get 12 different view angle images.

*C. Convolution Procedure*

With the help of Gabor application we created 12 different 2-D Gabor masks $\mathcal{G}(x, y)$, $(x, y)\ \epsilon\ \Omega$, we convolved our input image $I(x, y)$, to get a Gabor featured image $r(x, y)$ as follows;

$$r(x, y) = \iint_{\Omega} I(\xi, \eta) * g(x - \xi, y - \eta) \tag{11}$$

This formulation gives us 12 different representation of inputted image, corresponding to each angle discuss in eq. 2 and each of the element (cytoplasmic) which image consists of, have all possible view angle representation ($0°\ to\ 360°$). This way we are able to plot every cytoplasmic element in 3-D representation. Next, a Gaussian low-pass filter was applied to this magnitude image, with the purpose of reducing its variance and, consequently, reducing the classification error.

*D. Combining all convolved images*

The outputs of convolving procedure in each image point can be combined in a single quantity (textured image) that is called Gabor energy. That energy simply formulated by finding out final covariance matrix from all convolved images. This feature is related to the model of a specific type of orientation selective neuron in the primary visual cortex and is defined in the following way;

$$\mathcal{G}_{energy(L_{1i})} = \sum_{i=2p+1}^{12} C_i(j) * C_{i+1}(k + 1 - j) \tag{12}$$

This formulation accounts for all the covariance matrix which we for convolved in level 1 step 4 (figure 1) eq. 12 returns 6 covariance matrix form 12 convolved images. In the level 2 step 5 (figure 1) we repeat this process until we get final covariance image. *Where*, $p = 0, 1, 2, \ldots, 5$ i.e. $i$ will keep track all convoluted images ($1\ to\ 12$). Let m is the length of $C_i$ and n is the length of $C_{i+1}$, than the length of $\mathcal{G}_{energy}$ $m + n - 1$ whose $K^{th}$ element is displayed in eq. 12 and the sum is over all the values of $j$ which lead to legal subscripts for $C_i(j)$ and $C_{i+1}(k + 1 - j) : \min(k, m)$. When $m = n$.Next two steps can be formulated as follows;

$$\mathcal{G}_{energy(L_{2i})} = \sum_{i=2p+1}^{6} L_{1i}(j) * L_{1(i+1)}(k + 1 - j) \tag{13}$$

*Where*, $p = 0, 1, 2$ i.e. $i$ will track all convoluted image($1\ to\ 6$)

$$\mathcal{G}_{energy(L_{3i})} = \sum_{i=2p+1}^{3} L_{2i}(j) * L_{2(i+1)}(k + 1 - j) \tag{14}$$

*Where*, $p = 0, 1$ i.e. $i$ will track all the convoluted images ($1\ to\ 6$) and *finally*, we Conquer all these convoluted images (from convolution process) in the one covariance matrix (classification) this entire process gives us final segmented image. The images resulting from this filtering process served as variables or input texture bands in a supervised classification process using the maximum likelihood method.

So the figure 2 shows the abstract view of all the process which leads us to concluded texture image.

This all process can we judge by this mathematics;

$$Final\ Textured\ Image = covn^{1}[\sum_{i=1}^{12} \mathrm{IM} * GM_i] \quad (13)$$

Where IM = input image that would remain constant until the final corresponding (Texture) image, (*) convolution operator, GM = Gabor mask (eq. 1), $covn^{1}$ defines that final outcome contains final covariance matrix. Later part shows the discussion with doctors (only subjectivity). In the next paper we try to proof grading analysis (I, II, III), means in which grade our input image lies and compare it by doctor's prognosis regarding grading.

Later this textured image has been passed from level set formulation phase where these differences among intensities are plotted with different color in the purpose of segmenting the each cytoplasmic element distinctly. This level set formulation deforms iteratively to partition the image into region. Main idea behind this approach is that to distinguish background and fore ground (biased region and cytoplasmic part).

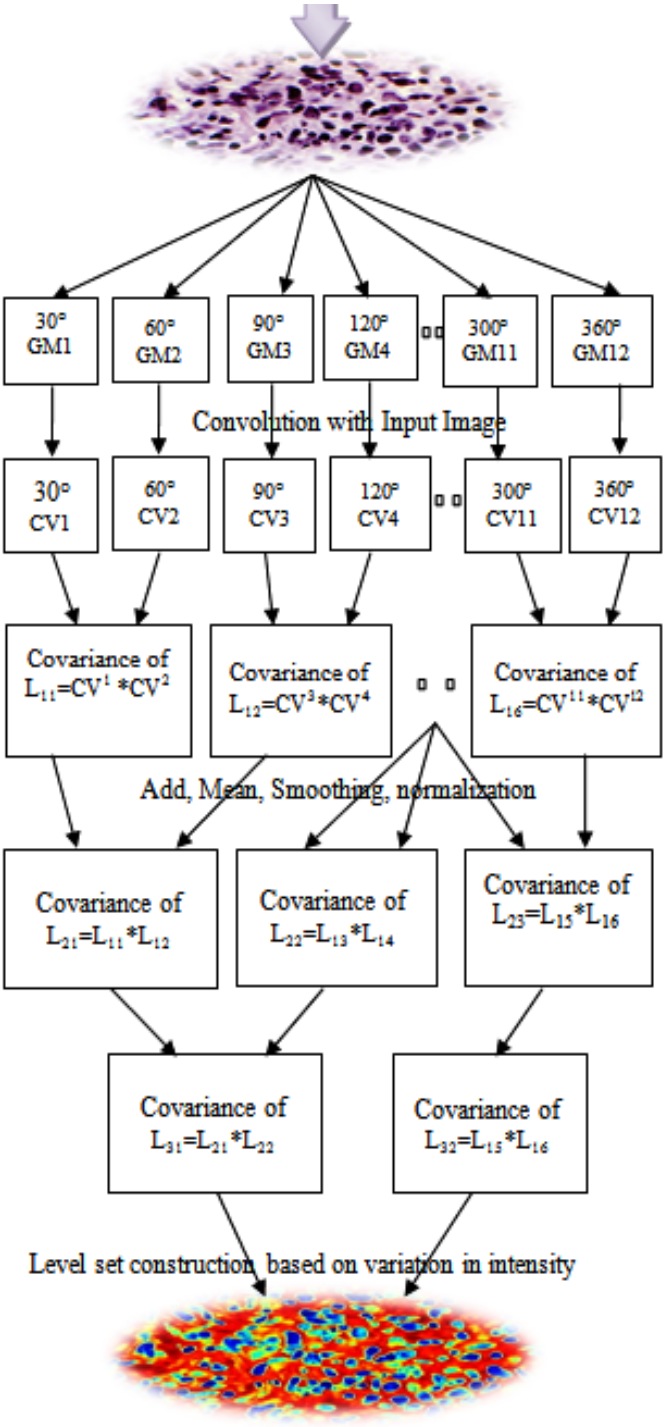


**Figure 2.** Final output textured Image

In this level set frame work, contour $C$ is in 2-Dimensional plane (coming from Gabor application) simple embedded in a 3-Dimensional surface $\phi$, this $\phi$ will track inside ($\phi < 0$) and outside ($\phi > 0$) when $\phi$ crosses a plane at the 0 level. This $\phi$ is chosen to be the signed distance function (SDF) such that; the $|\phi|$ is equal to the distance from $x$ to the closest point on contour $C$ and interior points have a negative sign. This choice is made so that we can cluster homogeneous intensities and

distinguished on account of color, where intensity varies drastically.

The level sets may be deformed in order to minimize some segmentation energy. We use one of the popular Chan-Vese energy to trace the contour from given imagery;

$$E^{cv} = \int_{inside} (I - \mu_1)^2 + \int_{outside} (I - \mu_2)^2 \qquad (14)$$

This Chan-Vese energy has following evolution equation;

$$F = (I - \mu_1)^2 + (I - \mu_2)^2 \qquad (15)$$

In this following evolution *F* should only be computed along the zero level set and should be normalized such that $|\phi| < 0.5$ at each iteration.

*Updating $\phi$ near the zero level set*:

Once *F* has been computed and normalized, we follow up the same procedure that Swan Lankton [34] has apply to update $\phi$ along the zero level set as well as the four other lists of adjacent points. Note the use of five additional lists that temporarily hold that are changing status:

$$S_0 = S_z \xrightarrow{emplies} points\ moving\ to\ L_0$$

$$S_{-1} = S_{n1} \xrightarrow{emplies} points\ moving\ to\ L_{-1}$$

$$S_1 = S_{p1} \xrightarrow{emplies} points\ moving\ to\ L_1$$

$$S_{-2} = S_{n2} \xrightarrow{emplies} points\ moving\ to\ L_{-2}$$

$$S_2 = S_{p2} \xrightarrow{emplies} points\ moving\ to\ L_2$$

These five lists are summarized as follows;

A. Primarily, scan through $L_0$ list and add the corresponding value of *F* to the existing value of $\phi$ at each point.

B. Points where the new value of $\phi$ is outside the range [-.5, .5] are removed from $L_0$ and added to $S_{-1}$ or $S_1$ according to denote that they will be changing status to $L_{-1}$ or $L_1$ respectively.

C. List $L_{-1}$ *and* $L_1$ are scanned and $\phi$ values are updated so that they are exactly 1 unit form their nearest neighbor in $L_0$. If no $L_0$ neighbor exists, the point is moved to $S_{-2}$ or $S_2$ respectively.

D. Points in $L_{-1}$and $L_1$ whose update $\phi$ value fall outside of the specified range for $L_{-1}$ or $L_1$ are moved to $S_0$, $S_{-2}$, or $S_2$ respectively.

E. List $L_{-2}$ and $L_2$ are scanned and $\phi$ values are updated so that they are exactly 1 unit from their nearest neighbor in $L_{-1}$ *or* $L_1$. If no $L_{-1}$ or $L_1$ neighbors exists, the point is removed from all the lists, and the value of $\phi$ and the label map is changed to $-3$ to $+3$ accordingly.

F. Points in $L_{-2}$ and $L_2$ whose update $\phi$ value is outside of the specified range are removed from $L_{-2}$ or $L_2$ and either moved $S_{-1}$or $S_1$ if their value is too low, or removed from all lists if their value is too high. Points that are removed from all the lists should have corresponding points in $\phi$ and the label map is changed to $-3$ to $+3$ accordingly.

Once all points in the list $L_0$,$L_{-1}$, $L_1$, $L_{-2}$, $L_2$ have been visited, it is necessary to process points that have changed status during the iteration. This is describing in following points;

*Updating list during iteration*

A. Scan $S_0$. Move each point onto $L_0$ and update the value of the label map to 0.

B. Scan $S_{-1}$ and $S_1$. Move point onto $L_{-1}$ or $L_1$ accordingly and update the label map to -1 or 1. If the point on $L_{-1}$ or $L_1$ have neighbors with $\phi$ values equal to -3 or +3, add the neighbor to the appropriate $S_{-2}$ or $S_2$lists while setting their $\phi$ value to be 1 unit from the value of current point.

C. Scan $S_{-2}$ and $S_2$ move each point onto $L_{-2}$ or $L_2$ accordingly and update the label map to -2 0r 2 depending on the sign.

By running above both procedure (updating $\phi$near the zero level set and updating list during iteration) a full iteration is completed and F can be re-computed based on the new position of the contour. This process is repeated until convergence is reached.

With the help of this process we are able to get our final textured outcome figure 2. (c) & (f) and figure 3. (k) & (n) respectively.

## V. Experimental Result's and Discussion

To capture the desired result, we partitioned the images into distinct cytological components using an unsupervised segmentation. Typically in H&E stained FL & NB images, there are five major components, i.e., nuclei, cytoplasm, background, red blood cells (RBCs) and extracellular material and each of them is expressed in hues of different colors. At the segmentation step, we used the L*a*b* color space, where the difference between two colors are perceptually uniform; therefore the Euclidean distance can be used as a measure [6]. In figure 2 image (g) & (h) explains the amount of area coverage by each cytoplasmic component because this classification is needed at a time of prognosis of tissue sample. Discussion with doctors leads us to know about the relevance of these cytoplasmic components in the occurrence of diseased grading. They suggested us any single tissue made up nuclei surrounded by cytoplasm, and usually nuclei is round in shape, but when the patients suffer from lymphomas, nuclei shape deteriorate (either reduce in size or become larger from actual), result more and less cytoplasm and nuclei occurrence in textured image. We have taken two images (figure 2 (a) & (d)) of follicular lymphoma grade II and III, respectively and other two of neuroblastoma (figure 3 (i) & (l)) in ours 170 images of database. Discussion with doctors helps us to understand each cytological component and plot each of them distinctly with different color.

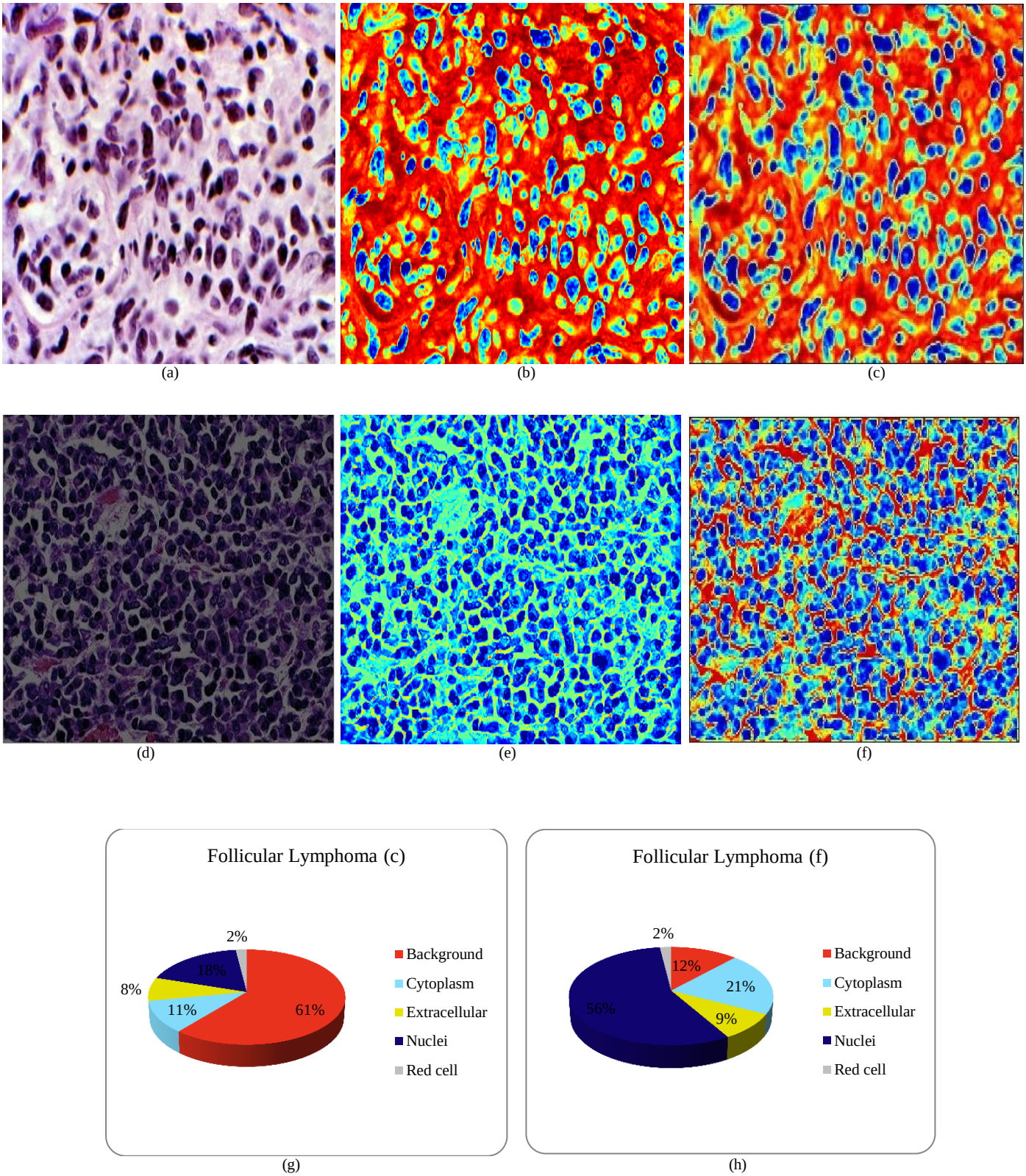


**Figure 3.**(a) & (d) are the input images of Follicular Lymphoma Grade II & III respectively, (b)& (e) are the intermediary result of texture segmentation, (c) & (f) are the final outcome of segmentation, (g) & (h) are shows amount of cytoplasmic component present in the final output image.

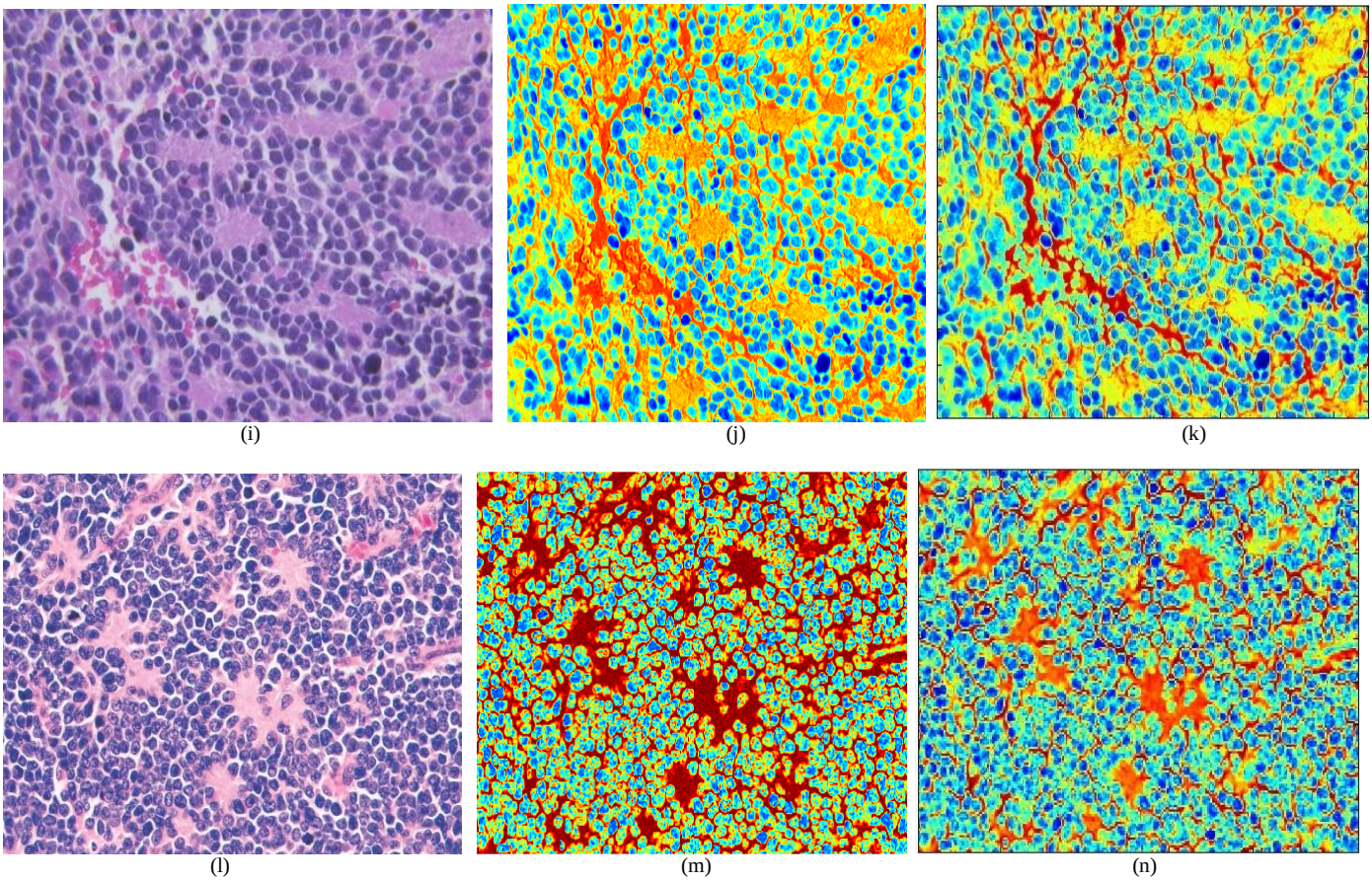


**Figure 4.** (i) & (i) are the input images of Neuroblastoma both belong to Unfavorable Histology, (j) & (m) are the intermediary result of texture segmentation, (k) & (n) are the final outcome of segmentation, (o) & (p) are shows amount of cytoplasmic component present in the final output image.

Though this discussion is confined to qualitative criterion of grading of Lymphomas, still this study can provide a healthy discussion regarding grading of lymphomas because In figure 2 (images (g) & (h)) and in figure 3 (images (o) & (p)) quantized each cytoplasmic component, level set formulation maintain a lists for accounting each cytoplasmic element separately. This quantization provides doctors additional input with minimal cost help to make efficient decision timely and also helps in the categorization into respective grades as CB/HPF ratio can we visualized. Moreover occurrence of cytoplasmic component (mainly nuclei, cytoplasm) classified neuroblastomic

lymphomas in to Favorable and Unfavorable stromal classification.

Sample H&E-stained images (shown in figure 2 (a) & (d)) and their segmentation (Textured) results (shown in figure 2 (c) & (f)) of Follicular Lymphoma, each color represent its own identity blue corresponds to nuclei, cyan to cytoplasm yellow to extracellular and red and gray to background and red cells, respectively.

Sample H&E-stained images (shown in figure 3 (i) & (l)) and their segmentation results(shown in figure 3 (k) & (n)) of Neuroblastoma, each color represent its own identity Blue corresponds to nuclei, cyan to cytoplasm yellow to extracellular and red and gray to background and red cells, respectively. We could also able to differentiate the low intermediate and high grades (CB/HPF) with reasonable accuracies.

In previous researches segmentation based on color [14] are not much more effective for the image having high CB/HPF ratio the displayed it outcomes in gray scale (black & white). Those out comes hardly justify our grading scheme of H&E stained histopathological image.

## VI. Conclusion

We introduced a novel approach color texture analysis method and applied it for computer-aided prognosis of Follicular Lymphoma and Neuroblastoma images. Gaussian wavelet orientation transformation of color images prior to Co-occurrence calculation for H&E-stained histopathological images considerably improved the classification performance, which has 97% sensitivity in identifying according to pathologist for follicular lymphoma. Our proposed method demonstrates great promise in establishing structural, color-textural, in histopathological images of FL & NB. Moreover our classification approach gives additional input to pathologist so that patients should receive appropriate therapy as soon as possible to increase their chance of re-mission and to prolong their lives. It should be noted that the automated computer assisted grading system should never be considered a replacement for pathologist. Instead, it should only be used as assistance to the decision mechanism. In case of a disagreement between the computerized system and the doctors rating, the final decision is that of the human doctors (pathologist), we will see these following scenarios in our future aspect,

- The proposed color texture analysis approach is also applicable to analyze other kinds of images with limited color spectrum and this will be investigated.
- To count the number of nuclei and other Centro blast element present in any image and also demarking them appropriate manner for visualization purpose.

**REFERENCES**


[1] American Cancer Society 2011. http://www.cancer.org

[2] Siddharth Samsi, Gerard Lozanski, Arwa Shana'ah, Ashok K. Krishanmurthy, Metin N. Gurcan [Senior Member, IEEE] "Detection of Follicles from IHC Stained Slides of Follicular Lymphoma Using Iterative Watershed", *IEEE Trans Biomed Eng*. vol. 57, no. 10, pp. 2609–2612, 2010.

[3] Jaffe, E.S., Harris, N.L., Stein, H., and Vardiman, J.W., "Tumors of Hematopoietic and Lymphoid Tissues", *IRAC Press*, Lyon, 2001.

[4] Clausi, D.A & M.E. Jernigan, "Designing Gabor filters for optimal texture separability". *Pattern Recognition*. Vol. 33, pp. 1835-1849, 2000.

[5] Bovic, A.C., 1991. "Analysis of multichannel narrowband filters for image texture segmentation". *IEEE Transactions on signal processing*. Vol. 39 no. 9, pp. 2025-2043, 1991.

[6] G. Paschos, "Perceptually Uniform Color Spaces for Color Texture Analysis: An Empirical Evaluation," *IEEE Trans. On Image Processing*, pp. 932-937, 2001.

[7] Metin N. Gurcan, Senior Member, IEEE, Laura Boucheron, Member, IEEE, Ali Can, Member, IEEE, Anant Madabhushi, Member, IEEE, Nasir Rajpoot, and Bulent Yener, Senior Member, IEEE, "Histopathological Image Analysis: A Review" *Department of Biomedical Informatics, the Ohio State University*, Columbus,OH 43210 USA, 2009.

[8] Jorge A. Recio, Luis A. Ruiz Fernan, "Use of Gabor filters for texture Classification of digital images" *ISSN: 0214-4557.Física de la Tierra*, vol. 17, pp. 47-59, 2005.

[9] Olcay Sertel, Jun Kong, Gerard Lozanski, Arwa Shana'ah, Umit Catalyurek, Joel Saltz, Metin Gurcan, "Texture Classification Using Nonlinear color Quantization: Application To histopathological Image". ICASSP, 2008.

[10] Oscar Nestares, Rafael Navarro, Javier Portilla and Antonio Tabernero , "Efficient Spatial-Domain Implementation Of A Multiscale Image Representation Based On Gabor Functions," *J electronic imagining* vol. 7, pp. 166-173, 1998.

[11] Swerdlow, S., Campo, E., Harris, N., Jaffe, E., Pileri, S., Stein, H., Thiele, J., and Vardiman, J., eds., "WHO classification of tumours of haematopoietic and lymphoid tissues", vol. 2, World Health Organization, Lyon, France, fourth ed. (2008).

[12] Basak Oztana, Hui Kongb, Metin N. Gurcanb, and B¨ulent Yenera, "Follicular Lymphoma Grading using Cell-Graphs and Multi-Scale Feature Analysis", *Proc. of SPIE* Vol. 8315 831516-1.

[13] Xuimei Zhang and Brian A. wandell, "A Spatial Extension of CIELAB for Digital Color Image Reproduction", *Stanford*, CA 94305.

[14] Amanpreet Kaur Bhogal, Neeru Singla, Maninder Kaur, "Color Image Segmentation Based On Color And Texture properties", *international journal of advanced engineering sciences & technologies* vol no.8,issue no.2,152-156.

[15] A. Rosenfeld and A. Kak, "Digital picture Processing," vol. 1, Academic Press, 1982.

[16] M. Levine, "Vision in Man and Machine," McGraw-Hill 1985.

[17] A. Teuner, O. Pichler and B. Hosticks, "Unsupervised Texture Segmentation of Images Using Tuned Matched

Gabor Filter," IEEE Transaction Image Processing vol. 4 no. 6, pp. 863-870, 1995.
[18] P. Cohen, C. Ledinh and V. Lacasse, "Classification of Natural Texture by Means of Two-Dimensional Orthogonal Masks," IEEE transaction Acoustic, Speech and Signal Processing, vol. 37 no. 1, pp. 125-128, 1989.
[19] A. Jain and F. Farrokhnia, "Unsupervised Texture Segmentation Using Gabor Filters," Patterns Recognition, vol. 24 no. 12, pp. 1167-1186, 1991.
[20] D. Dunn, W. Higgins and J. Wakeley, "Texture Segmentation Using 2-D Gabor Elementary Function," IEEE transaction Patterns Analysis and Machine Intelligence, vol. 17 no. 2 pp. 130-149, 1994.
[21] J. Bigun and J. du Buf, "N-folded Symmetries by Complex Moments in Gabor Space and Their Application to Unsupervised Texture Segmentation," IEEE Transaction Patterns Analysis and machine Intelligence, vol. 16 no. 1 pp. 80-87, 1994.
[22] A. Blake and A. Zisserman, "Visual Reconstruction," The MIT press, 1987.
[23] B. Povlow and S. Dunn, "Texture Classification Using Non-causal Hidden Markov Models," IEEE transaction Pattern Analysis and Machine Intelligence, vol. 17 no. 10, pp. 1010-1014, 1995.
[24] S. German and D. Geman, "Stochastic Relaxation, Gibbs Distribution and the Bayesian Restoration of Images," IEEE Transaction pattern Analysis and Machine Intelligence, vol. 6 no. 11, pp. 721-741, 1984.
[26] M. Hassner and J. Sklansky, "The Use of Markov Random Field as Models of Texture," Image Modelling, A. Rosenfeld (Ed.), Academic Press pp. 185-198 1981.
[26] H. Derin and H. Elliot, "Modeling and Segmentation of Noisy and Textured Images Using Gibbs Random Fields," IEEE Transaction pattern Analysis and Machine Intelligence, vol. 9 no. 1, pp. 395-407, 1987.
[27] M. Gurelli and L. Onural, "On a Parameter Estimation Method for Gibbs-Markov Fields," IEEE Transaction Patterns Analysis and Machine Intelligence, vol. 16 no. 4, pp. 424-430, 1994.
[28] H. Yin and N. Allinson, "Unsupervised Segmentation of texture of texture Images Using a Hierarchical Neural Structure," Electronics Letters vol. 30 no. 22, pp. 1842-1843, 1994.
[29] P. Andrey and P. Tarroux, "Unsupervised Segmentation of Markov Random Field Modelled Textured Images Using Selectionists Relaxation," IEEE Transaction Patterns Analysis and machine Intelligence, vol. 30 no. 3, pp. 252-262, 1998.
[30] D. Panjwani and G. Healey, "Markov Random Field Models for Unsupervised Segmentation of Textured Color Images," IEEE Transaction Pattern Analysis and Machine Intelligence, vol. 17 no.11, pp. 939-954, 1995.
[31] J. Bennett and A. Khotanzad, "Multispectral Random Field Models for Synthesis and Analysis of Color Images," IEEE Transaction Patterns Analysis and Machine Intelligence, vol.20 no. 1, pp. 327-332, 1998.
[32] A. Speis and G. Healey, "An Analytical and experimental Study of the Performance of Markov Random Fields Applied to Textured Images Using Small Samples," IEEE Transaction Image Processing vol. 5 no. 3, pp. 447-458, 1996
[33] S Krishnamachari and R. Chellappa, "Multiresolution Gauss-Markov Random Field Models for Texture Segmentation," IEEE transaction Image Processing, vol. 6 no. 2, pp. 251-267, 1997.
[34] Swan linkon, "Sparse Field Method: A technical report", PHD thesis report, 2009.
[35] G. Anneke, B. Bouwer, G. W. Imhoff, R. Boonstra, E. Haralambieva, A. Berg, B. jong, " Follicular Lymphoma grade 3B includes 3 cytogenetically defined subgroups with primary t(14;18), 3q27, or other translations: t(14;18) and 3q27 are mutually exclusive" blood journal hematology library, Feb. 2013.
[36] P. Brodatz, "Texture- A photographic Album for Artist and Designers," Dover, 1966.
[37] D. Dunn and W. Higgins, "Optimal Gabor Filters for Texture Segmentation," IEEE transaction on Image processing vol. 4 no. 7, pp. 947-964, 1995.
[38] T. Chan and L. Vese, "Active contours model without edges," IEEE transaction Image Processing, Vol. 10, no. 2, pp. 266-277, Feb. 2001.
[39] O. Sertel, J. Koga, H. Shimada, U. V. Catalyurek, J. H. Salyz and M. N. Gurcan, "Computer-aided Prognosis of Neuroblastoma on Whole-slide Image: Classification of Stromal Development," pattern recognition, pp. 1093-1103, 2009.
[40] S. Yhann and T. Young, "Boundary Localization in Texture Segmentation," IEEE Transaction Image Processing vol. 4 no. 6 pp. 849-856, 1995.
[41] Y. Hu and T. Dennis, "Textured Image Segmentation by Context Enhanced Clustering" IEEE transaction proceeding- Visual Image and Signal Processing, vol. 141 no. 6, pp. 413-421, 1994.
[42] Pranshu Saxena and Sanjay K. Singh, "Noble Approach for Texture Classification of H&E Stained Histopathological Image by Gaussian Wavelet," IEEE symposium intelligent system designs (ISDA) pp. 323-327 Nov 2012.
[43] Sonal Kothari, John H Phan, Andrew N Young and May D Wang, "Histological image classification using biologically Interpretable shape-based features," Kothariet al. BMC Medical Imaging, 2013,

## Author Biographies

**Pranshu Saxena,** received the B. E. degree in Information Technology from University of Pune, Pune, India in 2010, the M. Tech. degree in Computer Science Engineering from Lovely Professional University, Jalandhar, India in 2013.
His research interests include medical image processing, automated image segmentation, Image texture analysis and intelligent system. He has served as reviewer and committee member for a number of international conferences and journals in image processing, and medical imaging.

**Sanjay Kumar Singh** received the B. Tech and M. tech Degree from ABV-Indian Institute of Information Technology and Management, Gwalior in Information Technology in 2011. His research interests include medical image processing, Speech Signal Processing and Intelligent System.

**Prateek Agrawal** received the B. Tech degree from Agra college Agra in computer science engineering in 2007 and M. tech Degree from ABV-Indian Institute of Information Technology and Management, Gwalior in Software engineering in 2009. His research interests include Software engineering, Soft computing, Speech Signal Processing and Intelligent System.